water

MDPI

Article

Spatial and Temporal Assessment of Baseflow Based on Monthly Water Balance Modeling and Baseflow Separation

Huawei Xie [1,2], Haotian Hu [1,2], Donghui Xie [3], Bingjiao Xu [1,2], Yuting Chen [4], Zhengjie Zhou [5], Feizhen Zhang [6] and Hui Nie [1,2,*]

[1] College of Hydraulic and Environmental Engineering, Zhejiang University of Water Resources and Electric Power, Hangzhou 310018, China; xiehw@zjweu.edu.cn (H.X.); 2021b20037@stu.zjweu.edu.cn (H.H.); 2021b20045@stu.zjweu.edu.cn (B.X.)
[2] Key Laboratory for Technology in Rural Water Management of Zhejiang Province, Hangzhou 310018, China
[3] Ningbo Yuanshui Company Limited, Ningbo 315000, China
[4] Zhejiang Water Conservancy Development Planning Research Center, Hangzhou 310012, China; chenyt@zjwater.gov.cn
[5] Zhejiang Institute of Hydraulics & Estuary (Zhejiang Institute of Marine Planning and Design), Hangzhou 310020, China; zzjwater@163.com
[6] Hangzhou Nanpai Engineering Construction Management Service Center, Hangzhou 310020, China; hzzfz2005@163.com
* Correspondence: nieh@zjweu.edu.cn

Abstract: Baseflow is the part of streamflow that is mainly replenished by groundwater. The protection of the biological environment and the growth of its water resources greatly depend on the spatial and temporal evolution of baseflow. Therefore, the Baizhiao (BZA) and Shaduan (SD) catchments of the Jiaojiang River Basin (JRB) in the Zhejiang province of China were selected as study areas. The ABCD model and Eckhardt method were used to calculate baseflow and baseflow index (BFI). The temporal and spatial evolution patterns of baseflow were analyzed through statistical analysis and the Mann–Kendall test. The results showed that the ABCD model performs well in simulating overall hydrological processes on the monthly streamflow at BAZ and SD stations with NSE (Nash–Sutcliffe Efficiency) values of 0.82 and 0.83 and Pbias (Percentage Bias) values of 9.2% and 8.61%, respectively. The spatial–temporal distribution of the BFI indicates the higher baseflow contribution in upstream areas compared to downstream areas at both stations. The baseflow and BFI had significant upward trends at the BZA and SD stations in the dry season, while their trends were not uniform during the wet period. These findings are essential guidance for water resource management in the JRB regions.

Keywords: monthly-scale hydrological modeling; baseflow simulation; ABCD model; Eckhardt method; spatial and temporal analysis

Citation: Xie, H.; Hu, H.; Xie, D.; Xu, B.; Chen, Y.; Zhou, Z.; Zhang, F.; Nie, H. Spatial and Temporal Assessment of Baseflow Based on Monthly Water Balance Modeling and Baseflow Separation. *Water* **2024**, *16*, 1437. https://doi.org/10.3390/w16101437

Academic Editor: Adriana Bruggeman

Received: 18 March 2024
Revised: 11 May 2024
Accepted: 11 May 2024
Published: 17 May 2024

1. Introduction

Baseflow is a relatively stable streamflow component, mainly originating from subsurface streamflow or delayed portions of streamflow [1–3]. Baseflow can provide the necessary support for streamflow replenishment [4] and play a crucial role in supplementing groundwater in the basin [5]. Current global climate change and human activities have increased uncertainty in the hydrological cycle [6,7]. Many studies have analyzed the response of streamflow to climate change and human activities [8,9]. As a relatively stable water source, baseflow is essential in mitigating the impacts of seasonal and climatic variations on water resources [10,11]. A better understanding of groundwater replenishment and discharge processes can be achieved through temporal and spatial baseflow analysis, supporting the scientific and rational utilization of groundwater resources [12]. Therefore, gaining in-depth insights into the temporal and spatial evolution patterns of

baseflow in watersheds is crucial for maintaining ecological flow [13,14], managing water resources [15], and studying the patterns of drought evolution [16–18].

Currently, scholars use various baseflow simulation methods [19–21], mainly including numerical simulation methods [22,23], isotope methods [24], and water balance methods [25]. For example, Song et al. [26] quantitatively assessed the contributions of direct streamflow and baseflow to nitrogen loading in the Western Lake Erie Basins in China using numerical simulation methods, which can provide critical information for regional water resource management. Fillo et al. [24] used isotopic techniques to investigate how lawn watering affected baseflow in Denver, USA. They investigated the effects of lawn irrigation on baseflow in semiarid metropolitan regions and concentrated on examining the isotopic ratios of water molecules. Murray et al. [27] conducted an in-depth analysis of monthly baseflow trends in watersheds within Canada using the water balance method. This study aimed to explore the effects of climate change on baseflow, providing critical insights into the changes in hydrological cycles in Canada.

Water balance models can estimate relationships such as precipitation, snowmelt, evaporation, streamflow, and groundwater recharge [28]. The ABCD model, as a four-parameter hydrological model, uses precipitation and potential evapotranspiration as inputs to estimate changes in evapotranspiration, streamflow, soil moisture, and groundwater storage [29]. These four variables play crucial roles in simulating the hydrological processes of a watershed. Model parameter calibration is essential in applying the ABCD model, optimizing model parameters based on observed data to improve predictive accuracy. Standard parameter calibration methods include trial and error by Bayesian methods [30–32], which effectively adjust model parameters to adapt to the characteristics of different watersheds [33–35].

The choice to study the Jiaojiang River Basin is motivated by its significant importance for water resource management and ecological conservation despite facing challenges such as insufficient mainstream monitoring stations and lacking hydrological data for sub-watersheds. In recent years, the basin has experienced water scarcity due to the impacts of climate change and human activities. Therefore, this research aims to apply the monthly water balance four-parameter hydrological model (ABCD model) to (a) calculate streamflow in data-scarce watersheds, (b) simulate baseflow in each sub-watershed, and (c) assess the temporal and spatial evolution patterns of baseflow within the watershed. This study also aims to (d) provide a more scientific basis for future water resource management and ecological conservation as a powerful tool for technical support for regional water resource assessment and management.

2. Materials and Methods

2.1. Study Area

The JRB is one of the eight essential river basins in the Zhejiang Province, China. It borders the East China Sea to the east and is situated between 120°17′6″ E to 121°41′00″ E longitude and 28°32′2″ N to 29°20′29″ N latitude, covering an area of 6603 km^2 [36], as shown in Figure 1. The basin falls within a subtropical monsoon climate zone characterized by four seasons, mild temperatures, and abundant rainfall. The average annual precipitation is 1652 mm, and the average evaporation is 1237.9 mm (observed using a φ20 cm evaporation pan). Precipitation distribution is higher in mountainous areas than plains, with the southern part receiving more rainfall than the northern part. The southwestern and northwestern mountainous regions have the highest precipitation, while the lowest precipitation occurs in the coastal plain area of JRB. In recent years, water scarcity in the Jiaojiang River Basin has been caused by climate change and human activities. Therefore, studying the temporal and spatial evolution patterns of baseflow within the basin can offer technical support for regional water resource assessment and management.

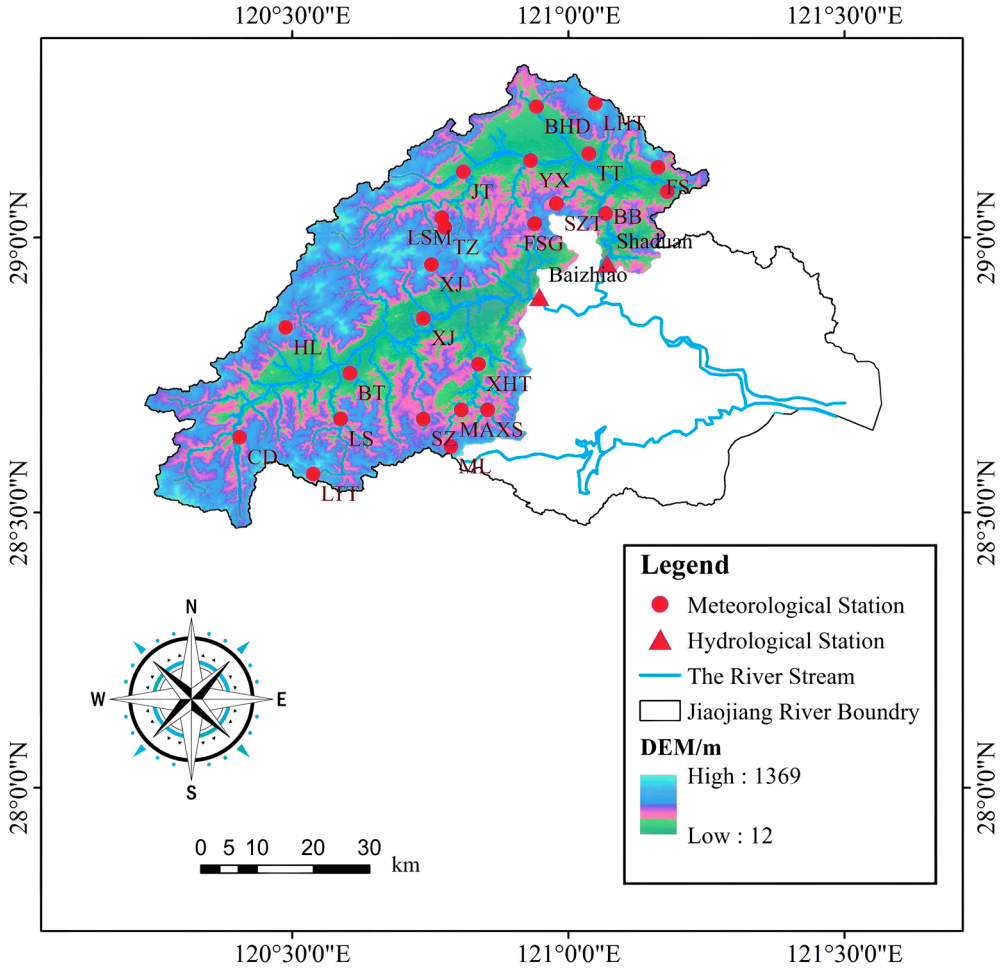

Figure 1. Schematic of the study area.

2.2. Data

This study selected streamflow data from two hydrological stations, namely, BZA and SD, in the JRB and conducted an analysis. The chosen data period for both stations is unified from 1990 to 2020. The daily precipitation and evaporation pan observation data for 24 meteorological stations within the JRB used in this study were sourced from the China Meteorological Science Data Sharing Service website (http://data.cma.cn, accessed on 1 May 2021).

2.3. Methodology

This study employed the Eckhardt [37] method for separating streamflow to obtain baseflow. The simulation of baseflow results is evaluated based on the BFI. Streamflow was simulated based on the ABCD model, and the temporal and spatial baseflow evolution patterns were analyzed through statistical analysis and the Mann–Kendall test [38], as shown in Figure 2.

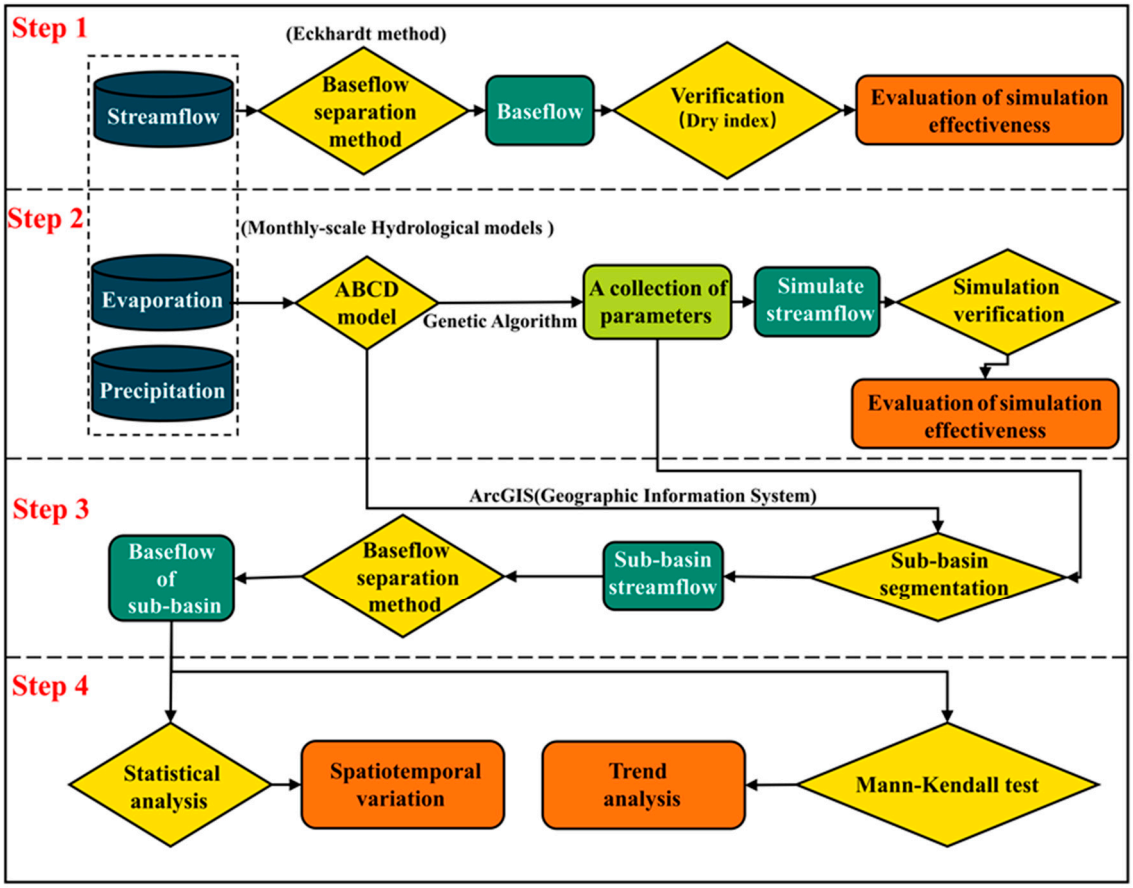

Figure 2. Study methodology flow chart.

2.3.1. Baseflow Separation Using Digital Filtering Method

The digital filter distinguishes between high-frequency and low-frequency signals because the rapid response qualities of direct streamflow are comparable to high-frequency signals, while the sluggish response characteristics of baseflow are similar to low-frequency signals [39]. Streamflow processes can be divided into direct and baseflow according to this split. Eckhardt [37] developed a general form for some filtering techniques, such as the Chapman–Maxwell method [39] and Lyne–Hollick approach [40], building on earlier research on digital filtering techniques.

$$b_i = Ab_{i-1} + By_i \tag{1}$$

In the equation, b_i represents the baseflow for time i, y_i represents the total net flow for time i, and A and B are functions of the recession coefficient α.

Assuming a linear relationship between the outflow and storage of the aquifer, the coefficients A and B can be expressed in terms of two variables: the recession coefficient (α) and the maximum BFI ($BFImax$). A more universally applicable digital filtering equation is obtained through derivation, known as the Eckhardt Digital Filtering Method.

$$b_t = \frac{(1 - BFI_{max})\alpha b_{t-1} + (1 - \alpha)BFI_{max}Q_t}{1 - \alpha BFI_{max}} \tag{2}$$

where α is the filtering parameter, BFI_{max} is the maximum of BFI, and Q_t is the measured streamflow at time t.

According to the research findings of Eckhardt, the parameter BFI_{max} can take empirical values under different hydrogeological conditions: for unconsolidated porous aquifers with perennial rivers, BFI_{max} is taken as 0.80; for unconsolidated porous aquifers with

seasonal rivers, *BFImax* is taken as 0.50; and for weakly permeable aquifers with seasonal rivers, *BFImax* is taken as 0.25. The value of α has a relatively small impact on the calculation results and can generally be set between 0.95 and 0.98.

To implement the Eckhardt method without conducting a hydrogeological investigation, Fan et al. [13] proposed a reverse filtering method using recession constants to calculate *BFImax*:

$$b_{t-1} = \frac{b_t}{\alpha}(b_t \leq Q_t) \tag{3}$$

Perform reverse iteration operations on daily flow based on the equation, and then obtain *BFImax* by dividing the maximum possible total baseflow by the total flow. Fan et al. [13] applied reverse filtering to generate different *BFImax* parameters for 1815 watersheds, which reflects the soil heterogeneity and the spatial variability of hydroclimatic variables.

2.3.2. Baseflow Index

The baseflow index (BFI) represents the contribution of baseflow to the total streamflow [41], and the following equation expresses it:

$$\mathrm{BFI} = \frac{\int_{t_1}^{t_2} Q_b(t)dt}{\int_{t_1}^{t_2} Q(t)dt} \tag{4}$$

where Q represents the total streamflow volume in cubic meters per second (m^3/s); Q_b is the baseflow volume in cubic meters per second (m^3/s); t is the time step; and t_1 and t_2 represent the starting and ending times, respectively.

2.3.3. The Low-Flow Index Method

The Low-Flow Index is an important indicator reflecting the characteristics of groundwater supply to river streamflow. Q_{90} and Q_{50} represent the flow rates occurring with frequencies equal to or greater than 90% and 50%, respectively. These flow rates are determined using the daily flow duration curve [42]. The product of the Low-Flow Index (Q_{90}/Q_{50}) and the annual total streamflow were taken as the observed value of the annual baseflow to compare with the above baseflow separation estimation results.

2.3.4. ABCD Model

The watershed storage area is conceptualized as layers of soil and groundwater according to the ABCD model [29] (Figure 3). Evapotranspiration losses happen when precipitation reaches the soil layer, and the amount of evapotranspiration varies with soil moisture content in a nonlinear empirical manner. There are two components to streamflow: baseflow is released from groundwater, and direct streamflow is the total surface streamflow, followed by subsurface flow from precipitation and soil water. Groundwater can be replenished by soil water seeping downhill. Many studies [31,32] have used the ABCD model to simulate watershed streamflow in various regions and have obtained good simulation accuracy.

Within a finite time step (monthly or yearly), the mass balance equation for soil water is:

$$S_i - S_{i-1} = P_i - E_i - R_i - D_i \tag{5}$$

where i represents the time step; S_{i-1} and S_i are the soil water storage at the beginning and end of the time step; and P_i, E_i, R_i, and D_i represent the precipitation, evapotranspiration, groundwater recharge, and direct streamflow within the time step, respectively.

In the ABCD model, the actual evapotranspiration (E) is a function of precipitation (P) and soil water storage (S) [29]. It defines two state variables for this purpose, namely, effective water content (W_i) and potential evapotranspiration (Y_i). They can be expressed by the following equations:

$$W_i = P_i + S_{i-1} \tag{6}$$

$$Y_i = E_i + S_i \tag{7}$$

Assuming a nonlinear functional relationship between Y_i and W_i, the following is established:

$$Y_i(W_i) = \frac{W_i + b}{2a} - \left[\left(\frac{W_i + b}{2a}\right)^2 - \frac{W_i b}{a}\right]^{0.5} \tag{8}$$

where both a and b are parameters. The range of a is $0 \leq a \leq 1$, reflecting the sensitivity of Y_i to changes in W_i, and b represents the maximum possible value of Y_i:

$$S_i = Y_i exp(E_{0i}/b) \tag{9}$$

where E_{0i} represents the potential evapotranspiration.

Utilizing Equations (3) and (4), Equation (1) can be rewritten as:

$$R_i + D_i = W_i - Y_i \tag{10}$$

For the allocation of R_i and D_i, the ABCD model further assumes:

$$\begin{cases} R_i = c(W_i - Y_i) \\ D_i = (1 - c)(W_i - Y_i) \end{cases} \tag{11}$$

where c is the third parameter of the model.

The ABCD model simplifies the groundwater layer as a linear reservoir, which can be expressed as:

$$F_i = dG_i \tag{12}$$

where d is the fourth parameter of the model.

Substituting Equation (9) into Equation (2), we obtain:

$$G_i = \frac{[c(W_i - Y_i) + G_{i-1}]}{(1 + d)} \tag{13}$$

Thus, the total streamflow of the watershed $Q_i = D_i + F_i$.

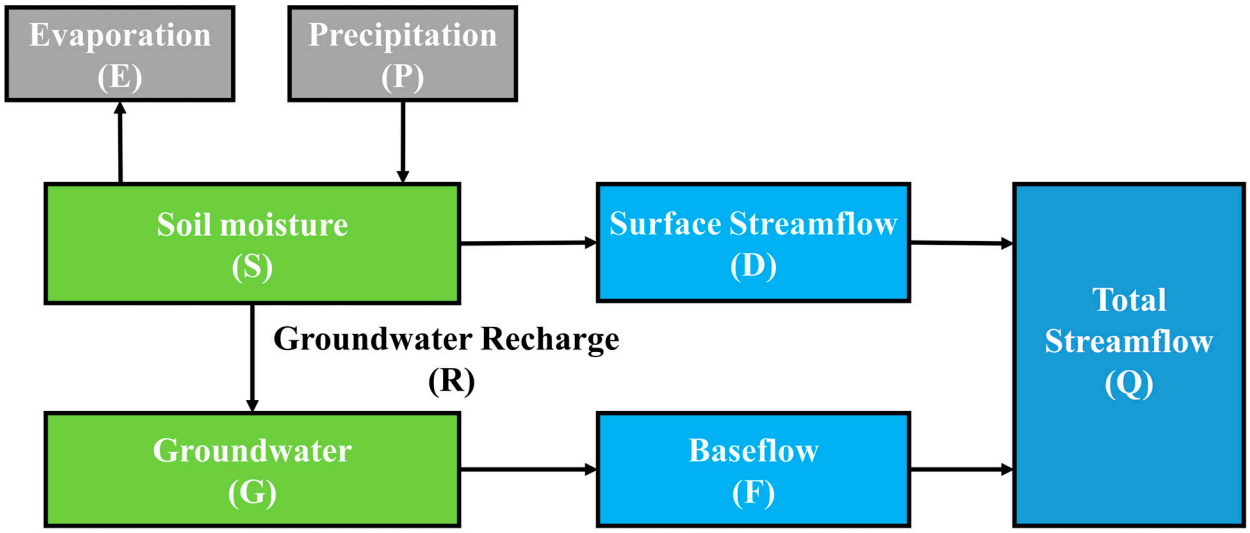

Figure 3. Conceptual diagram of the ABCD model.

2.3.5. Model Performance Evaluation

We employed a Genetic Algorithm (GA) for parameter calibration in this study. GA aims to find the optimal solution to a given problem, analogous to Darwin's theory of evolution, where individual traits are preserved in a population. GA preserves a candidate

solution set (also known as individuals) tailored to the specific problem. These candidate solutions are iteratively evaluated to create the next generation of solutions. Solutions with better traits are more likely to be selected and pass on their characteristics to the next generation of candidate solutions. As generations progress, the candidate solution set can better address the current problem.

We utilized GA to optimize the parameters of our model to maximize its fit with observed data. Initially, we defined a fitness function to assess the quality of each parameter set. We then initialized a population containing multiple parameter sets as candidate solutions. Subsequently, we iteratively evaluated these candidate solutions and selected the best based on their fitness values to generate the next generation. New solutions were created in each generation through crossover and mutation operations and added to the next generation's population. After multiple iterations, we obtained a set of optimized parameters that maximized the model's fit with the observed data.

The normalized dimensionless NSE (Nash–Sutcliffe Efficiency) [43] compares the variance of the measured and simulated data to determine the fit quality. The NSE value range is -1 to negative infinity. Better simulation results and increased model reliability are indicated by a higher NSE value closer to 1. On the other hand, a lower NSE value, nearer 0, denotes worse simulation outcomes with more significant modeling process mistakes, and the overall dependability of the simulation findings is reduced. The model is deemed untrustworthy if the NSE is noticeably less than 0.

Expressed mathematically as:

$$\mathrm{NSE} = 1 - \frac{\sum_{t=1}^{T}\left(Q_o^t - Q_m^t\right)^2}{\sum_{t=1}^{T}\left(Q_o^t - \overline{Q_o}\right)^2} \tag{14}$$

where Q_O refers to observed values, Q_m refers to simulated values, Q^t denotes a specific value at time t, and $\overline{Q_o}$ represents the overall mean of observed values.

The Percentage Bias (Pbias) [44] represents the percentage difference between the measured and simulated water flows compared to the corresponding inferred natural water flow. The closer the Pbias is to 0, the better the model performance.

$$\mathrm{Pbias} = \sum_{i=1}^{n} \frac{Q_{si} - Q_{oi}}{Q_{oi}} \times 100 \tag{15}$$

where Q_{oi} is the observed flow on the i-th day; Q_{si} is the simulated flow on the i-th day; Q_o is the mean observed flow for the days in question; and n is the length of observed data.

2.3.6. Mann–Kendall Test

The World Meteorological Organization suggests the widely used non-parametric Mann–Kendall test [38]. Since Mann and Kendall first put it forth, many studies have used it to examine patterns in time series data of various variables, including temperature, rainfall, streamflow, and water quality. The sample does not need to follow a particular distribution for the Mann–Kendall test to be valid, and it is unaffected by a small number of outliers. Computing appropriately for non-normally distributed data such as meteorological, hydrological, and other types is straightforward.

The null hypothesis H_0 in the Mann–Kendall test states that the time series data $X = (x_1, \ldots, x_n)$ is made up of n independent random variables with identical distributions. The alternative hypothesis H_1 is a two-sided test in which the distributions of x_k and x_j are different for every $k, j \leq n$, and $k \neq j$,. The test statistic S is calculated as follows:

$$S = \sum_{k=1}^{n} \sum_{j=k+1}^{n-1} sgn\left(x_k - x_j\right) \tag{16}$$

Here, $sgn()$ is the sign function, defined as follows:

$$sgn(x_k - x_j) = \begin{cases} 0 & (x_k - x_j) > 0 \\ 1 & (x_k - x_j) = 0 \\ -1 & (x_k - x_j) < 0 \end{cases} \quad (17)$$

The statistic S follows a normal distribution with a mean of 0, and the variance $Var(S)$ is calculated as follows:

$$Var(S) = \frac{n(n-1)(2n+5)}{18} \quad (18)$$

When $n > 10$, the standard typical statistic is calculated using the following formula:

$$Z = \begin{pmatrix} \frac{S-1}{\sqrt{Var(S)}} & S > 0 \\ 0 & S = 0 \\ \frac{S+1}{\sqrt{Var(S)}} & S < 0 \end{pmatrix} \quad (19)$$

If $Z > 1.96$ or $Z < -1.96$, at a significance level of $\alpha = 0.05$, we reject the null hypothesis H_0, indicating enough evidence to support the alternative hypothesis $H1$. If $-1.96 \leq Z \leq 1.96$, at a significance level $\alpha = 0.05$, we accept the null hypothesis H_0 [38].

3. Results and Discussions

3.1. Streamflow Simulation Using ABCD Model

The ABCD model parameters for the BZA and SD hydrological stations are shown in Table 1. The parameter values for the two neighboring basins are relatively close. Once the parameters and initial values were determined, the optimized model parameters were used to optimize the simulated flows from 1990 to 2010. In addition, the initial values of S and G were further optimized to obtain the best simulation results from 2011 to 2020. The correlation with measurements is shown in Figure 4. The simulated results for the BZA and SD hydrological stations have NSE values of 0.82 and 0.83, respectively, and Pbias values of 9.2% and 8.61%. The overall deviation of the water quantities derived from the ABCD model from the observations at the BZA and SD hydrological stations is positive, which suggests that the model slightly overestimates the actual observed values of the mean hydrological processes. The NSE is more than 0.8, and the Pbias is less than 10%, which indicates that the ABCD model is a good fit and can be used for hydrological simulation in JRB [45].

Table 1. The ABCD model parameters for two hydrological stations.

Station	A	B (mm)	C	D	Soil Water Storage (mm)	Groundwater Storage (mm)
BZA	0.98	220.43	0.37	0.72	50.64	578.29
SD	0.96	283.69	0.30	0.60	27.50	675.55

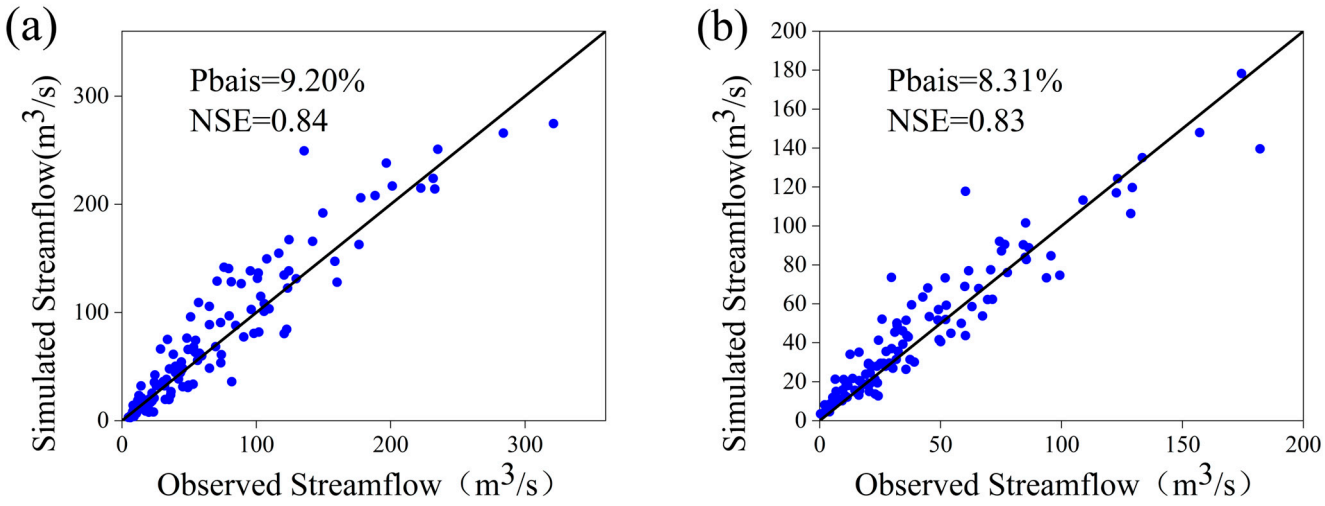

Figure 4. Scatter plot of observed and simulated monthly streamflow in the (**a**) BZA and (**b**) SD stations.

3.2. Baseflow Simulation Applying Eckhardt Digital Filtering Method

Table 2 illustrates the ABCD model parameters for the BZA and SD hydrological stations. There are slight differences in the parameter values between the two adjacent basins, with the parameter values for BZA consistently higher than those for SD. The parameters at the daily scale exhibit significant fluctuations in both basins. Hence, monthly scale parameters were adopted for excellent stability and reliability in modeling.

Table 2. Baseflow and streamflow characteristics at two hydrological stations.

Station	Average Daily Streamflow (m^3/s)	Average Daily Baseflow (m^3/s)	Maximum Daily Baseflow (m^3/s)	Median Daily Baseflow (m^3/s)	Average Monthly Streamflow (m^3/s)	Average Monthly Baseflow (m^3/s)	Monthly Maximum Baseflow (m^3/s)	Median Monthly Baseflow (m^3/s)
BZA	71.55	35.92	396.14	22.73	70.99	35.82	158.42	28.48
SD	39.33	21.81	195.80	15.31	41.36	21.72	85.72	16.82

The baseflow simulation was conducted for the SD and BZA watersheds using the ABCD model, followed by baseflow separation using the Eckhardt digital filtering method. To validate the baseflow separation estimation results, we used the product of the Low-Flow Index (Q_{90}/Q_{50}) and the annual total streamflow as the observed value of the annual baseflow. This observed value was compared with the baseflow calculated using the ABCD model. The NSE and Pbias were then used to validate the baseflow calculated by the ABCD model. Subsequently, the simulated results were evaluated using the observed streamflow multiplied by the low-flow index (Figure 5). The NSE values for baseflow simulation at the BZA and SD stations were 0.81 and 0.85, respectively. The Pbias values of baseflow simulation for the BZA and SD stations were 8.65% and 5.90%, respectively, indicating a slight underestimation of the observed values by the model. The baseflow separation results showed that this method could effectively simulate baseflow, which can provide a fundamental reflection of the annual variation within the watershed. Moreover, this approach could be utilized to analyze and research the spatiotemporal evolution of baseflow in the SD and BZA stations [46].

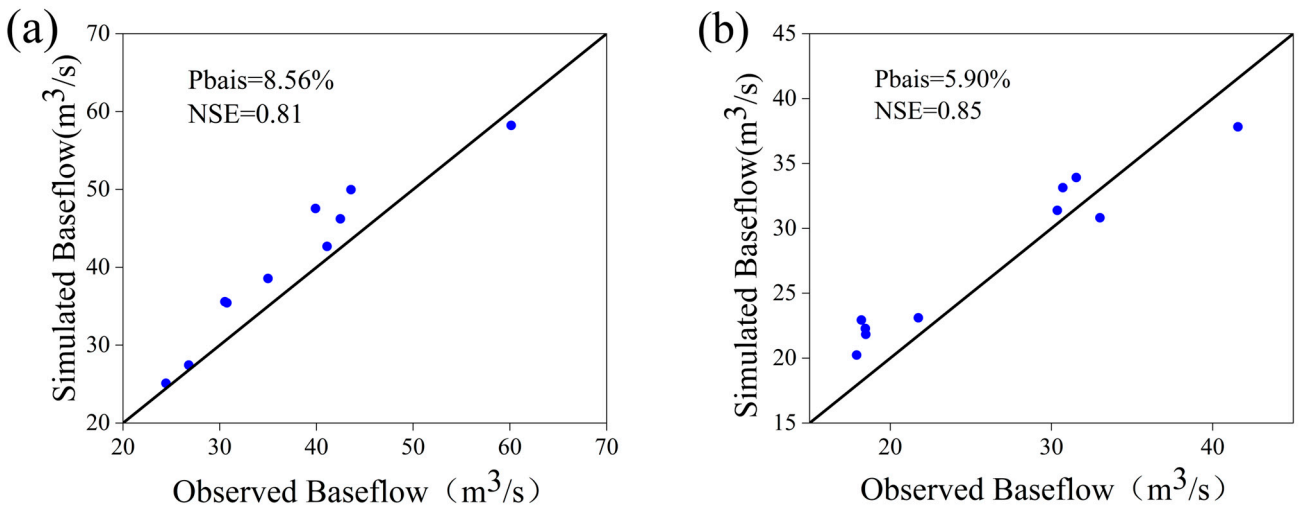

Figure 5. Watershed observation and simulation of yearly Baseflow verification in the (**a**) BZA and (**b**) SD stations.

3.3. Division of Wet and Dry Periods by BFI Value

Figure 6 illustrates the variation of monthly BFI based on the results of the digital filtering method to derive BFI values. The BFI variation pattern at the BZA and SD stations remained consistent throughout the year, with the maximum BFI occurring in December and the minimum in August. The flow in rivers decreased as the seasons changed and rainfall decreased. River replenishment has increasingly relied on subsurface runoff, which has increased the supply of subsurface runoff. Consequently, the BFI has increased as the percentage of subsurface runoff to river replenishment has decreased. This has resulted in an increase in groundwater recharge, which has decreased the amount of groundwater contributing to river flow and raised the BFI. During the summer, river recharge is primarily dependent on precipitation and groundwater. The groundwater input to river flow increases proportionately with rainfall, lowering the BFI [47].

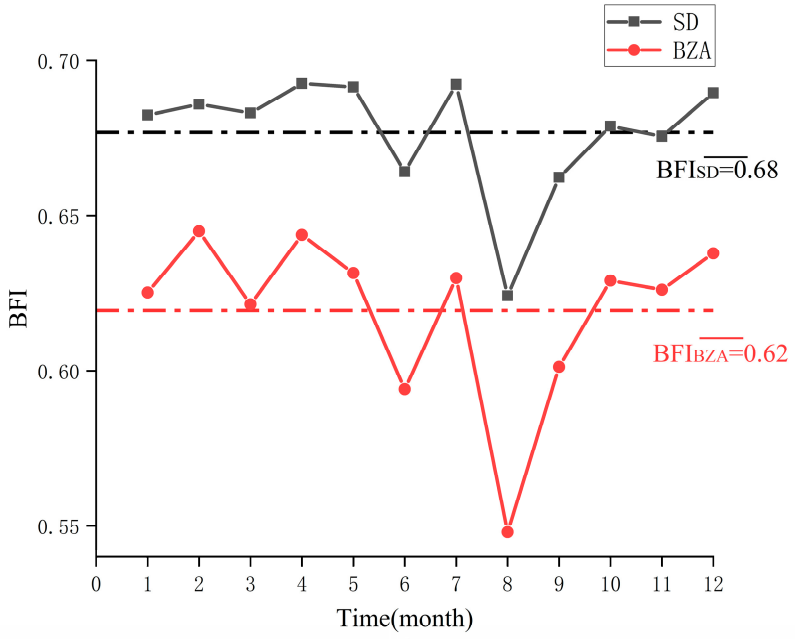

Figure 6. Monthly scale BFI changes at BZA and SD stations.

According to the monthly BFI results at the BZA and SD stations, the variation of monthly BFI is shown in Figure 7. By comparing multi-year average BFI values, the period from October to April was identified as the dry season, while May to September was considered the wet season for the watershed. As a result, the rainy season was defined as the months with BFI below average and the dry season as those with BFI above average [48].

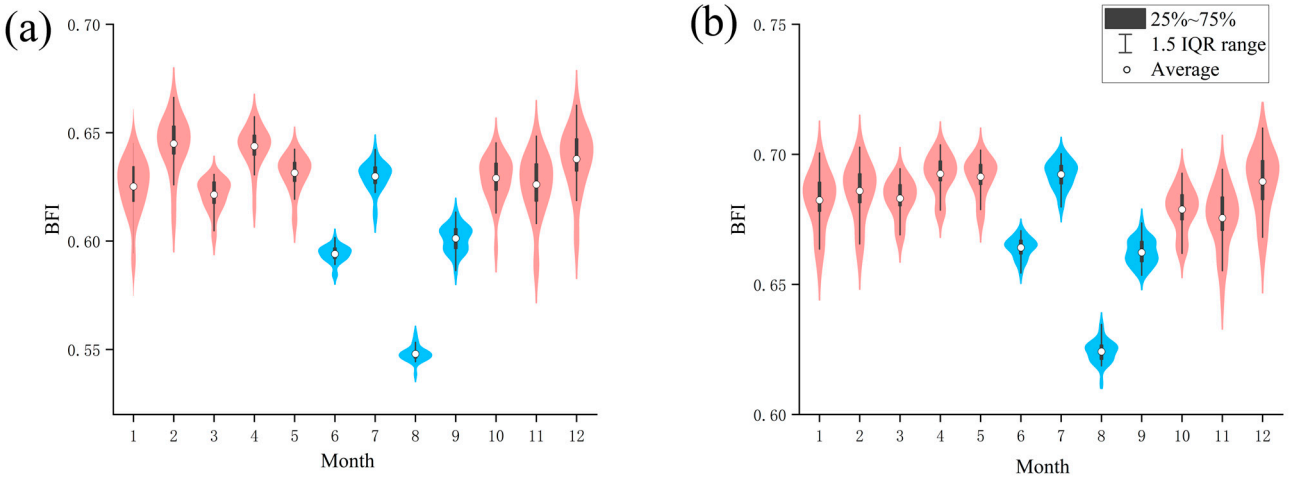

Figure 7. A comparison of BFI between wet and dry seasons for (**a**) BAZ and (**b**) SD stations. The red (blue) color represents dry (wet) season.

3.4. Spatial and Temporal Distribution Characteristics of Baseflow

The monthly baseflow and BFI statistical analysis for the BZA and SD watersheds from 1990 to 2020 are shown in Figure 8. As indicated in Figure 8, the BFI did not exhibit significant differences due to variations in watershed area, suggesting that the model performed well in capturing the baseflow process. The watershed area considerably impacted baseflow discharge, increasing baseflow as the area expanded. Numerous outliers in the baseflow for both BZA and SD suggested significant fluctuations in monthly flow rates [47].

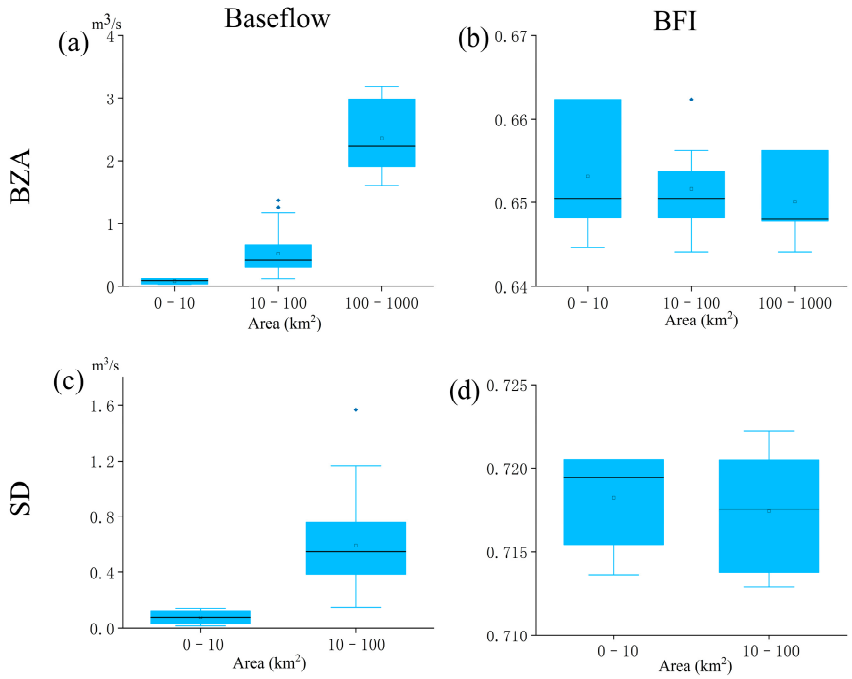

Figure 8. The boxplots of baseflow and BFI for (**a**,**b**) BAZ and (**c**,**d**) SD stations.

The baseflow in the JRB exhibited a significant geographical gradient trend, increasing from southwest to northeast. There was a notable gradient difference in baseflow among different regions within the basin, ranging from below 0.27 m^3/s to over 3.27 m^3/s. This may be attributed to the typically higher elevation or complex terrain in the southwest, which could have led to a more concentrated water flow, forming high-value areas of baseflow. Conversely, the lower terrain in the northeast may have resulted in relatively lower baseflow. The terrain gradient could have accelerated the flow of water, influencing the distribution of baseflow across different basin regions. The seasonal variations and distribution of precipitation in the subtropical monsoon climate could have induced spatial variations in baseflow. Monsoonal climates are often characterized by distinct wet and dry seasons, which may have contributed to differences in baseflow within the basin [44]. Higher terrain in the southwest might have been more susceptible to the influence of monsoon rains, while the northeast could have been relatively drier. WNW winds might have created differences in moisture transport within the basin, resulting in spatial variations in baseflow [46]. Specific wind directions might have transported moisture to specific areas of the basin, affecting precipitation and thus influencing baseflow formation. These factors collectively may have contributed to the spatial variation of baseflow within the basin.

Figure 9 showed the BFI, baseflow modulus, and average annual baseflow distribution for all Sub-watersheds at BZA and SD basins during all, wet, and dry seasons. The BZA watershed has a spatial trend in the baseflow modulus, with larger values in the upstream areas and smaller values in the downstream areas. The baseflow modulus in the upstream regions exhibits a broader range of fluctuations, ranging from 140 to over 220 (L/km·s), while it is relatively minor in the downstream areas. Geological conditions and hydrological processes in the upstream areas may have influenced the spatial differences in the baseflow modulus. However, the baseflow modulus was significant in upstream and downstream areas, with a relatively large fluctuation range maintained between 100 and 180 (L/km·s) in the SD watershed. The study suggests complex hydrological processes governing baseflow in the entire SD watershed. Factors such as relatively flat terrain similarly affect the basin's baseflow formation. With comparatively more significant values in the upstream areas ranging from below 0.66 to over 0.68, the BFI in the BZA watershed is generally smaller. By contrast, the BFI in the SD watershed is often more significant, fluctuating within an overall range of 0.68 to 0.74. Precipitation, evaporation, terrain, and other complicated elements within the basin may have impacted the spatial differences in the BFI among different locations [49–51].

Figure 10 illustrates the overall baseflow trend in the JRB. Both the BZA and SD areas exhibit significant increases in baseflow, with a slight increase in the baseflow index upstream of BZA and a slight decrease downstream. During the wet season, the baseflow in BZA generally decreases significantly, while the baseflow index in BZA increases significantly, and the SD area shows an overall significant decrease. In contrast, during the dry season, the baseflow and baseflow index in all areas exhibit significant increases. The trends of average baseflow discharge and BFI for all sub-basins during the wet and dry seasons indicate an annual increase in baseflow, suggesting the basin is building up groundwater reserves. Groundwater responds slowly to changes due to its lengthy recharging cycle. Therefore, the increase in baseflow can indicate substantial groundwater recharge in earlier periods, contributing to steady growth in groundwater reserves [52]. Furthermore, the yearly increase in the BFI has demonstrated an upward tendency in the baseflow proportion relative to the overall streamflow. Due to the subtropical monsoon climate and topography of the JRB, there may be a more significant percentage of groundwater recharging with total streamflow, as shown by this rise in the BFI. There were notable seasonal and regional variations in temperature and precipitation distribution.

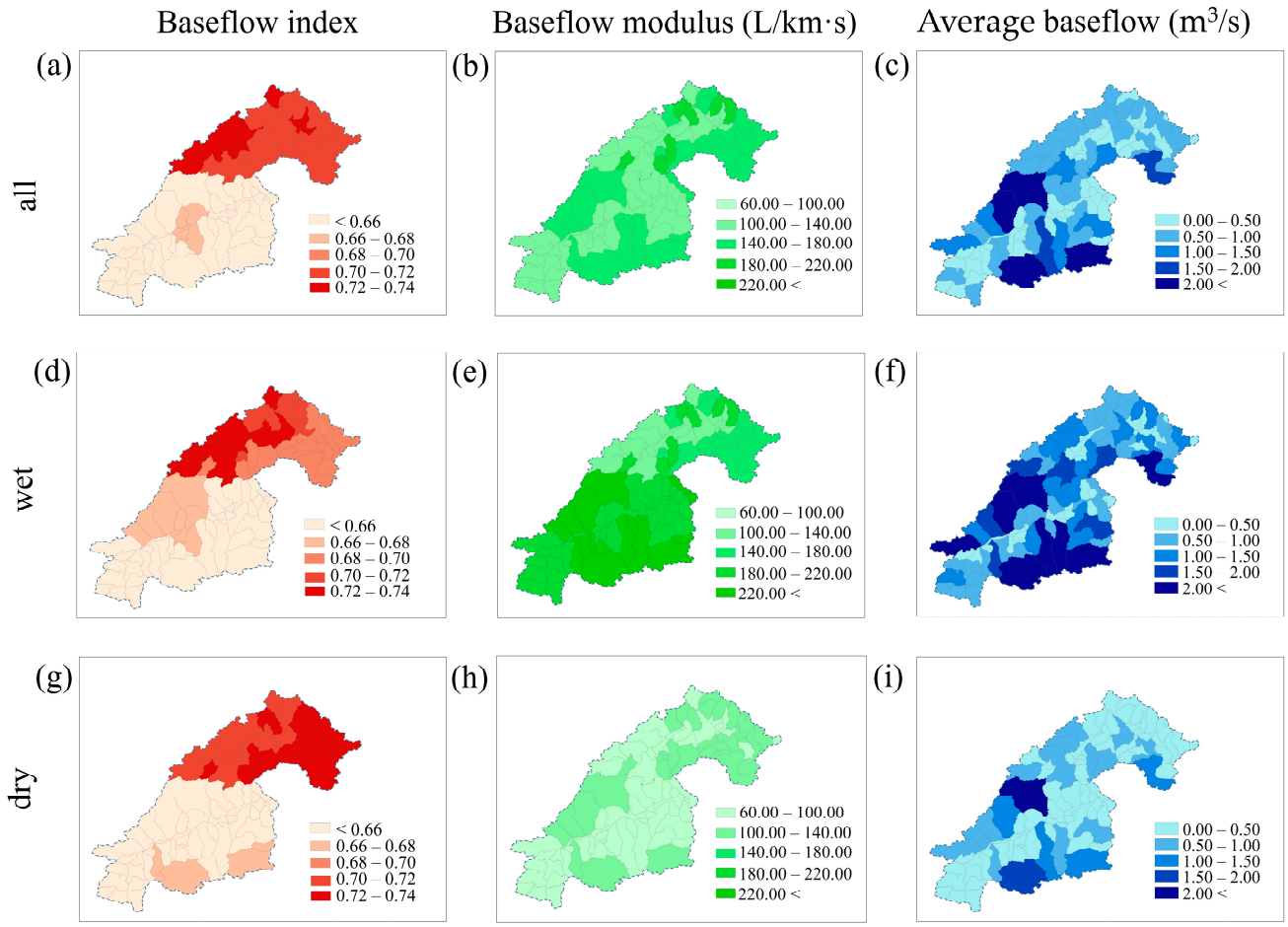

Figure 9. BFI, baseflow modulus, and average annual baseflow distribution for all Sub-Watersheds in (**a**–**c**) all seasons, (**d**–**f**) wet season, and (**g**–**i**) dry season.

Figure 11 illustrates the correlation analysis between evaporation, precipitation, and baseflow for all sub-basins. Surface runoff and groundwater infiltration may be impacted by changes in precipitation patterns and temperature distribution brought on by climate change. Long-term climate patterns may have increased groundwater recharge and baseflow generation. Groundwater recharge and circulation may have been significantly impacted by the basin's geological features [53]. Precipitation and baseflow are generally positively correlated, while the BFI is negatively correlated. The differences between the wet and dry seasons are not significant overall. Evaporation is generally positively correlated with the baseflow and BFI. During the wet season, evaporation negatively correlates with the baseflow and strongly positively correlates with the BFI. During the dry season, evaporation positively correlates with the baseflow and weakly positively correlates with the BFI. Overall, the baseflow in the BZA is more positively correlated with evaporation than in the SD. The SD area is generally more negatively correlated with the BFI than the BZA area. There is not much difference in the correlation of evaporation with the baseflow and the BFI between the two basins.

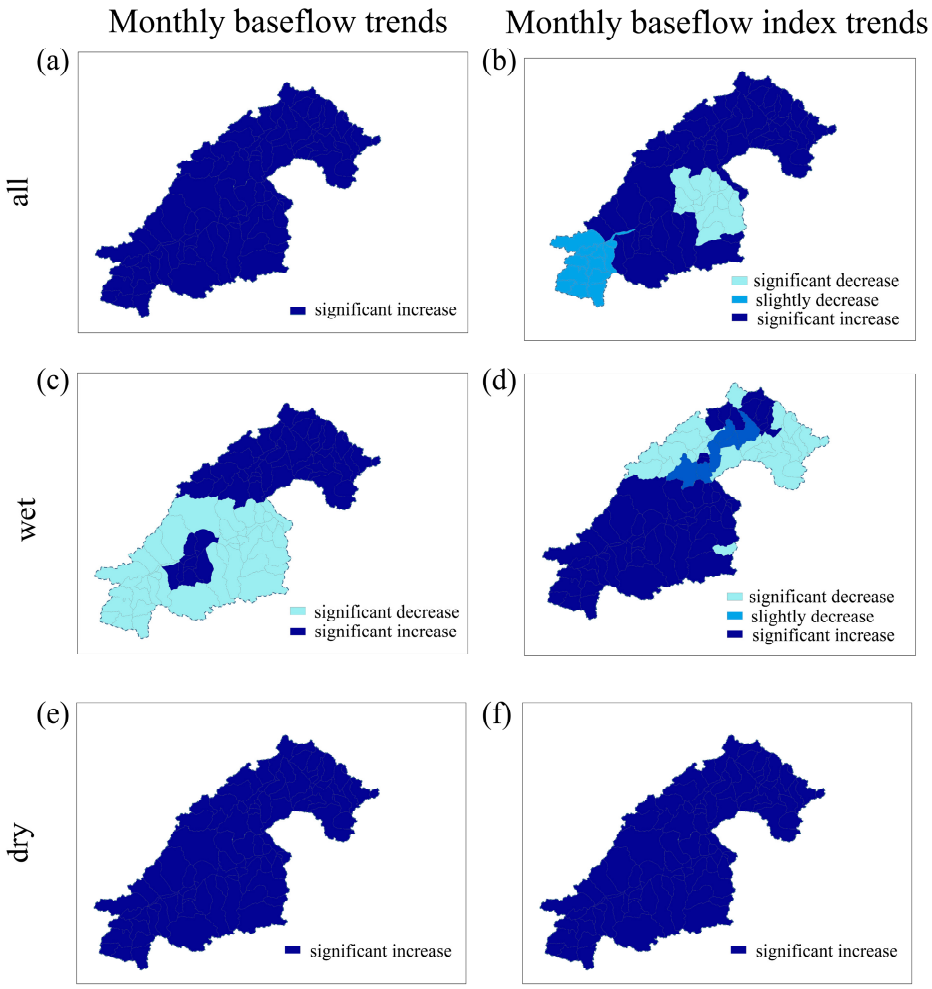

Figure 10. The trend distribution of average baseflow discharge, BFI, and baseflow modulus for all sub-basins in (**a**,**b**) all seasons, (**c**,**d**) wet season, and (**e**,**f**) dry season.

The genesis of baseflow may have been impacted by different groundwater flow patterns in the aquifers due to variations in the geological structure and rock types found in the JRB [51]. During the rainy season, baseflow increased somewhat, while the patterns varied by region. During this time, the BFI somewhat dropped, suggesting a decline in the proportion of groundwater in the overall streamflow. During the rainy season, there was a noticeable increase in streamflow discharge, which may have approached the maximum baseflow discharge. This implied that while the percentage of baseflow reduced during heavy rainfall, surface streamflow contributed comparatively more to the overall streamflow. Throughout the dry season, baseflow showed a significant increasing trend, whereas the rise of BFI remained pretty stable. One possible explanation for the sharp rise in baseflow during the dry season is a combination of reduced precipitation, comparatively low evapotranspiration, and steady groundwater recharging. The percentage of baseflow in the overall streamflow grew during this period, indicating the growing importance of groundwater in preserving the basin's hydrological balance [54].

The study is constrained by limited runoff data, which may introduce uncertainties in the simulation accuracy and the absence of measured baseflow data, leading to uncertainties in the baseflow simulation. Future research could include field experiments for validating baseflow simulations and conducting attribution analysis to identify critical factors, such as climate change and human activities, influencing baseflow changes in the watershed.

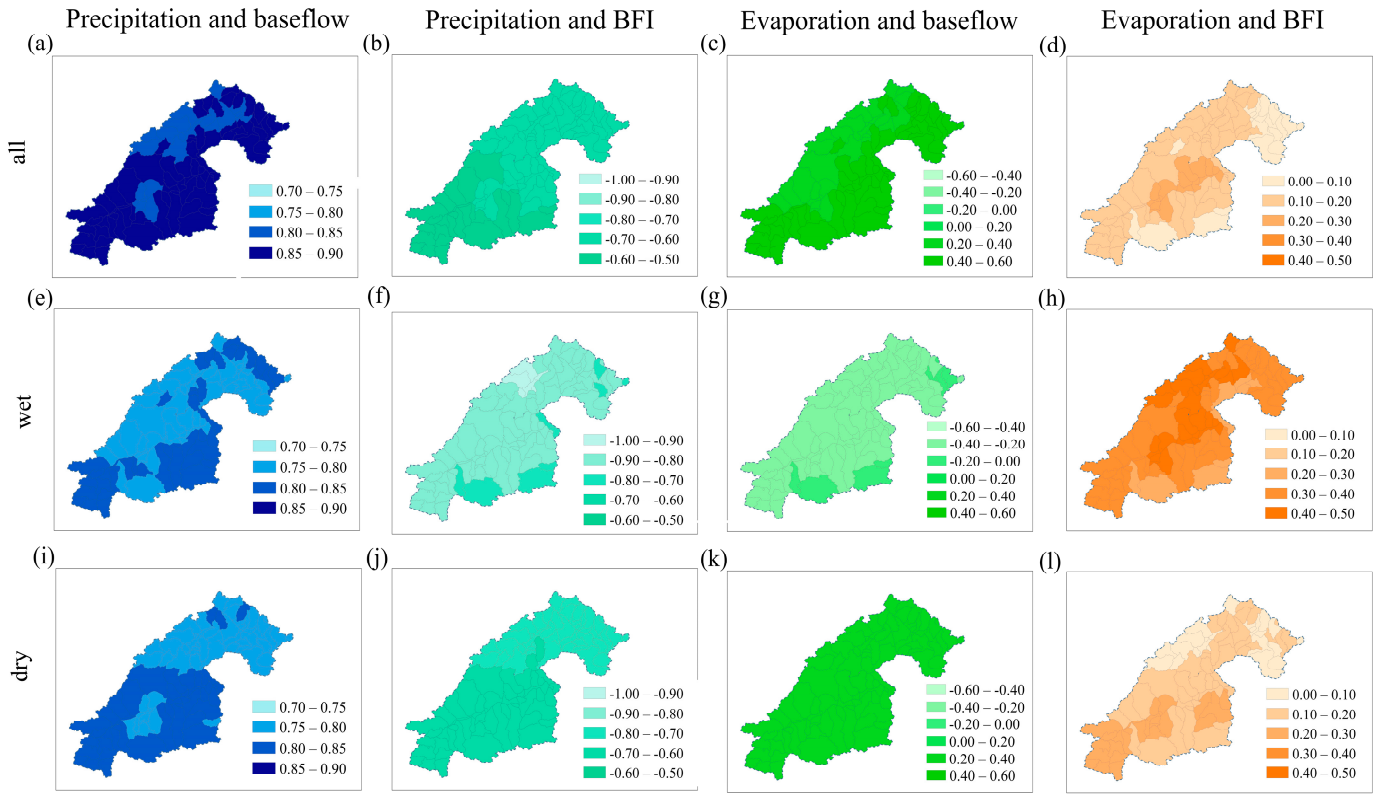

Figure 11. Correlation analysis between evaporation, precipitation, and baseflow for all sub-basins in (**a**–**d**) all seasons, (**e**–**h**) wet season, and (**i**–**l**) dry season.

4. Conclusions

This study utilized monthly streamflow data from the BZA and SD stations in the JRB to simulate baseflow (BFI) using the Eckhardt method and the ABCD model. In addition, it has achieved baseflow simulation in data-scarce basins based on a monthly scale hydrological model. The primary findings from this study are as follows:

(1) The simulated findings show that the NSE values for the BZA and SD stations are 0.82 and 0.83, and the Pbias values are 9.2% and 8.61%. According to available data, the ABCD model generally replicates monthly hydrological processes but overestimates the streamflow at the BZA and SD basins.

(2) Using the Eckhardt method to separate baseflow, the NSE values of baseflow simulations at the BZA and SD stations were 0.81 and 0.85, respectively. The Pbias values were 8.65% and 5.90%, respectively, which indicates that the model slightly overestimates baseflow in the BZA and SD stations. According to the BFI spatial distribution, there is a trend toward greater values in the upstream regions and lower values in the downstream regions. The BFI rises yearly, and the monthly hydrological model's baseflow exhibits a relatively fast expansion pattern.

(3) The increasing trends of baseflow were relatively small during the wet season but more significant during the dry season, highlighting the impact of seasonal variations on baseflow simulation in the monthly-scale hydrological model. The baseflow modulus in the upstream regions shows a broader range of fluctuations from 140–220 (L/km·s) and 100–180 (L/km·s) at the BZA and SD stations, respectively. Geological conditions and hydrological processes in the upstream areas may have influenced the spatial differences in the baseflow modulus.

This study provided a detailed analysis and validation for baseflow simulation in data-scarce basins using monthly-scale hydrological models. These findings are essential for gaining deeper insights into applying monthly-scale hydrological models in data-scarce

basins, scientifically managing water resources, providing environmental protection, and adapting to climate change.

Author Contributions: Conceptualization, D.X.; methodology, H.H. and Y.C.; software, H.H.; validation, H.H. and F.Z.; formal analysis, H.H., H.X. and D.X.; investigation, H.H., D.X. and Z.Z.; resources, Y.C. and B.X.; data curation, D.X.; writing—original draft preparation, H.H.; writing—review and editing, H.H., F.Z. and D.X.; visualization, H.H.; supervision, H.H.; project administration, H.N.; and funding acquisition, H.X. All authors have read and agreed to the published version of the manuscript.

Funding: This research was funded by the Zhejiang Provincial Water Resources Department Science and Technology Program, grant numbers RC2201 and RB2002; the Natural Science Foundation of Zhejiang Province, grant number LZJWY22E090007; and the Scientific Research Fund of the Zhejiang Provincial Education Department, grant number Y202352492.

Data Availability Statement: The daily precipitation and evaporation pan observation data for 24 meteorological stations within the JRB used in this study are sourced from the China Meteorological Science Data Sharing Service website (http://data.cma.cn, accessed on 1 May 2021).

Acknowledgments: We are grateful to the Zhejiang Hydrological Management Center for providing hydrological data.

Conflicts of Interest: Author Donghui Xie was employed by the company Ningbo Yuanshui Company Limited. The remaining authors declare that the research was conducted in the absence of any commercial or financial relationships that could be construed as a potential conflict of interest.

References

1. Chen, H.; Huang, S.; Xu, Y.P.; Teegavarapu, R.S.V.; Guo, Y.; Nie, H.; Xie, H. Using baseflow ensembles for hydrologic hysteresis characterization in humid basins of Southeastern China. *Water Resour. Res.* **2024**, *60*, e2023WR036195. [CrossRef]
2. Tallaksen, L.M. A review of baseflow recession analysis. *J. Hydrol.* **1995**, *165*, 349–370. [CrossRef]
3. Singh, S.K.; Pahlow, M.; Booker, D.J.; Shankar, U.; Chamorro, A. Towards BFI characterisation at national scale in New Zealand. *J. Hydrol.* **2019**, *568*, 646–657. [CrossRef]
4. Miller, M.P.; Buto, S.G.; Susong, D.D.; Rumsey, C.A. The importance of Baseflow in sustaining surface water flow in the Upper Colorado River Basin. *Water Resour. Res.* **2016**, *52*, 3547–3562. [CrossRef]
5. Niazi, A.; Bentley, L.R.; Hayashi, M. Estimation of spatial distribution of groundwater recharge from stream baseflow and groundwater chloride. *J. Hydrol.* **2017**, *546*, 380–392. [CrossRef]
6. Huntington, T.G. Evidence for intensification of the global water cycle: Review and synthesis. *J. Hydrol.* **2006**, *319*, 83–95. [CrossRef]
7. Pendergrass, A.G.; Knutti, R.; Lehner, F.; Deser, C.; Sanderson, B.M. Precipitation variability increases in a warmer climate. *Sci. Rep.* **2017**, *7*, 17966. [CrossRef] [PubMed]
8. Milly, P.C.; Dunne, K.A. Colorado River flow dwindles as warming-driven loss of reflective snow energizes evaporation. *Science* **2020**, *367*, 1252–1255. [CrossRef] [PubMed]
9. Vano, J.A.; Udall, B.; Cayan, D.R.; Overpeck, J.T.; Brekke, L.D.; Das, T.; Lettenmaier, D.P. Understanding uncertainties in future Colorado River streamflow. *Bull. Am. Meteorol. Soc.* **2014**, *95*, 59–78. [CrossRef]
10. Eltahir, E.A.B.; Yeh, P. On the asymmetric response of aquifer water level to floods and droughts in Illinois. *Water Resour. Res.* **1999**, *35*, 1199–1217. [CrossRef]
11. Peters, E.; Torfs, P.; Van Lanen, H.A.J.; Bier, G. Propagation of drought through groundwater—A new approach using linear reservoir theory. *Hydrol. Process.* **2003**, *17*, 3023–3040. [CrossRef]
12. Ciampittiello, M.; Dresti, C.; Saidi, H. Water resource management through understanding of the water balance components: A case study of a Sub-Alpine Shallow Lake. *Water* **2021**, *13*, 3124. [CrossRef]
13. Fan, Y.; Li, H.; Miguez-Macho, G. Global patterns of groundwater table depth. *Science* **2013**, *339*, 940–943. [CrossRef] [PubMed]
14. Poff, L.R.; Allan, J.D.; Bain, M.B.; Karr, J.R.; Prestegaard, K.L.; Richter, B.D.; Sparks, R.E.; Stromberg, J.C. The natural flow regime. *BioScience* **1997**, *47*, 769–784. [CrossRef]
15. Ebrahim, G.Y.; Villholth, K.G. Estimating shallow groundwater availability in small catchments using streamflow recession and instream flow requirements of rivers in South Africa. *J. Hydrol.* **2016**, *541*, 754–765. [CrossRef]
16. Sophocleous, M. Interactions between groundwater and surface water: The state of the science. *Hydrogeol. J.* **2002**, *10*, 52–67. [CrossRef]
17. Ahiablame, L.; Sheshukov, A.Y.; Rahmani, V.; Moriasi, D. Annual baseflow variations as influenced by climate variability and agricultural land use change in the Missouri River Basin. *J. Hydrol.* **2017**, *551*, 188–202. [CrossRef]
18. Beck, H.E.; Van Dijk, A.I.; Miralles, D.G.; De Jeu, R.A.; Bruijnzeel, L.A.; McVicar, T.R.; Schellekens, J. Global patterns in BFI and recession based on streamflow observations from 3394 catchments. *Water Resour. Res.* **2013**, *49*, 7843–7863. [CrossRef]

19. George, P.M.; Sekhar, M. Base flow simulation using a physically based subsurface model–The case of a tropical basin in the Western Ghats, India. *J. Hydrol.* **2022**, *613*, 128451. [CrossRef]
20. Luo, Z.; Shao, Q. A modified hydrologic model for examining the capability of global gridded PET products in improving hydrological simulation accuracy of surface runoff, streamflow and baseflow. *J. Hydrol.* **2022**, *610*, 127960. [CrossRef]
21. Longobardi, A.; Villani, P. Baseflow index characterization in typical temperate to dry climates: Conceptual analysis and simulation experiment to assess the relative role of climate forcing features and catchment geological settings. *Hydrol. Res.* **2023**, *54*, 136–148. [CrossRef]
22. Rumsey, C.A.; Miller, M.P.; Sexstone, G.A. Relating hydroclimatic change to streamflow, baseflow, and hydrologic partitioning in the Upper Rio Grande Basin, 1980 to 2015. *J. Hydrol.* **2020**, *584*, 124715. [CrossRef]
23. Welty, C.; Moore, J.; Bain, D.J.; Talebpour, M.; Kemper, J.T.; Groffman, P.M.; Duncan, J.M. Spatial heterogeneity and temporal stability of baseflow stream chemistry in an urban watershed. *Water Resour. Res.* **2023**, *59*, e2021WR031804. [CrossRef]
24. Fillo, N.K.; Bhaskar, A.S.; Jefferson, A.J. Lawn irrigation contributions to semiarid urban baseflow based on water-stable isotopes. *Water Resour. Res.* **2021**, *57*, e2020WR028777. [CrossRef]
25. Delesantro, J.M.; Duncan, J.M.; Riveros-Iregui, D.; Blaszczak, J.R.; Bernhardt, E.S.; Urban, D.L.; Band, L.E. The Nonpoint Sources and Transport of Baseflow Nitrogen Loading Across a Developed Rural-Urban Gradient. *Water Resour. Res.* **2022**, *58*, e2021WR031533. [CrossRef]
26. Song, J.H.; Her, Y.; Guo, T. Quantifying the contribution of direct streamflow and baseflow to nitrogen loading in the Western Lake Erie Basins. *Sci. Rep.* **2022**, *12*, 9216. [CrossRef] [PubMed]
27. Murray, J.; Ayers, J.; Brookfield, A. The impact of climate change on monthly baseflow trends across Canada. *J. Hydrol.* **2023**, *618*, 129254. [CrossRef]
28. Milly, P.C.; Betancourt, J.; Falkenmark, M.; Hirsch, R.M.; Kundzewicz, Z.W.; Lettenmaier, D.P.; Stouffer, R.J. Stationarity is dead: Whither water management? *Science* **2008**, *319*, 573–574. [CrossRef]
29. Thomas, H. *Improved Methods for National Water Assessment: Final Report*; U.S. Geological Survey: Reston, VA, USA, 1981; Volume 44. [CrossRef]
30. Wang, X.; Gao, B.; Wang, X. A modified ABCD model with temperature-dependent parameters for cold regions: Application to reconstruct the changing streamflow in the headwater catchment of the Golmud River, China. *Water* **2020**, *12*, 1812. [CrossRef]
31. Zou, Y.; Yan, B.; Feng, B.; Zhang, J.; Tang, Y.A. Three-Parameter Hydrological Model for Monthly Runoff Simulation—A Case Study of Upper Hanjiang River Basin. *Water* **2023**, *15*, 474. [CrossRef]
32. Leng, J.; Ma, K.; Gu, S.; Zhang, K.; He, D. A non-stationary impactquant framework for assessing the human activity impacts on hydrological drought in the Upper Red River. *Atmos. Res.* **2024**, *304*, 107419. [CrossRef]
33. Ghiggi, G.; Humphrey, V.; Seneviratne, S.I.; Gudmundsson, L. G-RUN ENSEMBLE: A multi-forcing observation-based global streamflow reanalysis. *Water Resour. Res.* **2021**, *57*, e2020WR028787. [CrossRef]
34. Do, H.X.; Gudmundsson, L.; Leonard, M.; Westra, S. The Global Streamflow Indices and Metadata Archive (GSIM)–Part 1: The production of a daily streamflow archive and metadata. *Earth Syst. Sci. Data* **2018**, *10*, 765–785. [CrossRef]
35. Hrachowitz, M.; Savenije, H.H.G.; Blöschl, G.; McDonnell, J.J.; Sivapalan, M.; Pomeroy, J.W.; Arheimer, B.; Blume, T.; Clark, M.P.; Ehret, U.; et al. A decade of Predictions in Ungauged Basins (PUB)—A review. *Hydrol. Sci. J.* **2013**, *58*, 1198–1255. [CrossRef]
36. Chen, H.; Huang, S.; Xu, Y.-P.; Teegavarapu, R.S.V.; Guo, Y.; Nie, H.; Xie, H.; Zhang, L. River ecological flow early warming forecasting using baseflow separation and machine learning in the Jiaojiang River Basin, Southeast China. *Sci. Total Environ.* **2023**, *882*, 163571. [CrossRef] [PubMed]
37. Eckhardt, K. How to construct recursive digital filters for baseflow separation. *Hydrol. Process.* **2005**, *19*, 507–515. [CrossRef]
38. Hamed, K.H.; Rao, A.R. A modified Mann-Kendall trend test for autocorrelated data. *J. Hydrol.* **1998**, *204*, 182–196. [CrossRef]
39. Chapman, T.G. Comment on "Evaluation of automated techniques for Baseflow and recession analyses" by RJ Nathan and TA McMahon. *Water Resour. Res.* **1991**, *27*, 1783–1784. [CrossRef]
40. Lyne, V.; Hollick, M. *Stochastic Time-Variable Rainfall-Streamflow Modelling*; Institute of Engineers Australia: Barton, Australia, 1979; Volume 79, pp. 89–93. Available online: https://www.researchgate.net/publication/272491803_Stochastic_TimeVariable_Rainfall-Streamflow_Modeling (accessed on 1 June 2022).
41. Chen, H.; Teegavarapu, R.S.V.; Xu, Y.-P. Oceanic-Atmospheric Variability Influences on Baseflows in the Continental United States. *Water Resour. Manag.* **2021**, *35*, 3005–3022. [CrossRef]
42. Ayers, J.R.; Villarini, G.; Jones, C.; Schilling, K. Changes in monthly baseflow across the US Midwest. *Hydrol. Process.* **2019**, *33*, 748–758. [CrossRef]
43. Nash, J.E.; Sutcliffe, J.V. River flow forecasting through conceptual models part I—A discussion of principles. *J. Hydrol.* **1970**, *10*, 282–290. [CrossRef]
44. Chen, H.; Xu, Y.P.; Teegavarapu, R.S.; Guo, Y.; Xie, J. Assessing different roles of baseflow and surface streamflow for long-term streamflow forecasting in southeastern China. *Hydrolog. Sci. J.* **2021**, *66*, 2312–2329. [CrossRef]
45. Baseri, M.; Mahjoobi, E.; Rafiei, F.; Baseri, M. Evaluation of ABCD water balance conceptual model using remote sensing data in ungauged watersheds (a case study: Zarandeh, Iran). *Environ. Earth Sci.* **2023**, *82*, 126. [CrossRef]
46. Martinez, G.F.; Gupta, H.V. Toward improved identification of hydrological models: A diagnostic evaluation of the "abcd" monthly water balance model for the conterminous United States. *Water Resour. Res.* **2010**, *46*, W08507. [CrossRef]

47. Bloomfield, J.P.; Gong, M.; Marchant, B.P.; Coxon, G.; Addor, N. How is Baseflow Index (BFI) impacted by water resource management practices? *Hydrol. Earth Syst. Sci.* **2021**, *25*, 5355–5379. [CrossRef]
48. Jiang, H.; Wang, Z.; Ye, A.; Liu, K.; Wang, X.; Wang, L. Hydrological characteristic-based methodology for dividing flood seasons: An empirical analysis from China. *Environ. Earth Sci.* **2019**, *78*, 399. [CrossRef]
49. Chen, S.; Ruan, X. A hybrid Budyko-type regression framework for estimating baseflow from climate and catchment attributes. *J. Hydrol.* **2023**, *618*, 129118. [CrossRef]
50. Saedi, J.; Sharifi, M.R.; Saremi, A.; Babazadeh, H. Assessing the impact of climate change and human activity on streamflow in a semiarid basin using precipitation and baseflow analysis. *Sci. Rep.* **2022**, *12*, 9228. [CrossRef] [PubMed]
51. Aboelnour, M.A.; Engel, B.A.; Frisbee, M.D.; Gitau, M.W.; Flanagan, D.C. Impacts of watershed physical properties and land use on baseflow at regional scales. *J. Hydrol. Reg. Stud.* **2021**, *35*, 100810. [CrossRef]
52. Hellwig, J.; Stoelzle, M.; Stahl, K. Groundwater and baseflow drought responses to synthetic recharge stress tests. *Hydrol. Earth Syst. Sci.* **2021**, *25*, 1053–1068. [CrossRef]
53. Tan, X.; Liu, B.; Tan, X. Global changes in baseflow under the impacts of changing climate and vegetation. *Water Resour. Res.* **2020**, *56*, e2020WR027349. [CrossRef]
54. Mo, C.; Ruan, Y.; Xiao, X.; Lan, H.; Jin, J. Impact of climate change and human activities on the baseflow in a typical karst basin, Southwest China. *Ecol. Indic.* **2021**, *126*, 107628. [CrossRef]